metals

MDPI

Article

Speciation and Behavior of Niobium in the Fe–Ti–O System: Localization, Isomorphic Substitution, and Microphase Enrichment

Turar Kusmanovich Sarsembekov [1,*], Tatyana Alexandrovna Chepushtanova [2], Yerik Serikovich Merkibayev [2], Rustam Khassanovich Sharipov [3] and Nauryzbek Bakhytuly [4]

1 BioMin Tech LLP, Ust-Kamenogorsk 070015, Kazakhstan
2 Mining and Metallurgical Institute, Department of Metallurgy and Mineral Beneficiation, Satbayev University, Almaty 050013, Kazakhstan; t.chepushtanova@satbayev.university (T.A.C.); y.merkibayev@satbayev.university (Y.S.M.)
3 Laboratory of Advanced Materials and Technologies, Kazakh-British Technical University, Almaty 050000, Kazakhstan; r.sharipov@kbtu.kz
4 Laboratory of Physical Methods of Analysis, The Institute of Metallurgy and Ore Beneficiation, Almaty 050010, Kazakhstan; nauka-phd@mail.ru
* Correspondence: t.sarsembekov@biomintech.kz; Tel.: +7-705-795-89-20

Abstract

Niobium commonly occurs as a minor component in Fe–Ti–O oxide systems associated with ilmenite ores and titanium-bearing metallurgical materials, yet its speciation and incorporation mechanisms remain insufficiently resolved. This study investigates the distribution, structural incorporation, and microphase localization of niobium in the Fe–Ti–O system, with emphasis on TiO_2-rich domains. Electron probe microanalysis with EDS/WDS, X-ray diffraction, thermal analysis, and thermodynamic modeling in HSC Chemistry were combined to characterize niobium-bearing phases in natural and model oxide systems. Niobium was found to occur in two principal modes: as a low-level isomorphic impurity in Fe–Ti oxide matrices and as localized enrichments in TiO_2-rich domains, particularly rutile lamellae. A first-order area-based estimate for representative analyzed grains suggests that approximately 60–80% of the detected niobium is associated with the lamellar TiO_2 channel. The combined observations are consistent with a sequential mechanism involving isomorphic substitution of Nb in Ti sites, followed by microphase enrichment and segregation into more compositionally distinct niobium-bearing oxide or titanate microphases. In the studied material, integrated mapped-field Nb is about 0.04 wt.%, whereas matrix Nb commonly lies at trace levels of about 0.02–0.05 wt.% under the applied analytical conditions, consistent with low-level background incorporation, whereas locally Nb-enriched rutile-like domains reach about 0.70–1.00 wt.%. TiO_2-rich domains are therefore identified as the principal concentrators of niobium in Fe–Ti oxide systems. Taken together, the natural observations, model experiments, and thermodynamic calculations support an integrated mechanistic sequence of Nb evolution in the Fe–Ti–O system: isomorphic substitution → microphase enrichment in TiO_2-related domains → segregation into distinct Nb-bearing oxides/niobates. These findings provide a practical framework for interpreting Nb behavior in natural and technological Fe–Ti–O materials.

Keywords: niobium; Fe–Ti–O system; ilmenite; rutile lamellae; isomorphic substitution; microphase enrichment; electron probe microanalysis

Check for updates

Academic Editor: Corby G. Anderson

Received: 13 April 2026
Revised: 9 May 2026
Accepted: 11 May 2026
Published: 19 May 2026

Copyright: © 2026 by the authors. Licensee MDPI, Basel, Switzerland. This article is an open access article distributed under the terms and conditions of the Creative Commons Attribution (CC BY) license.

1. Introduction

Niobium (Nb) belongs to the group of high-field-strength elements and is typically present in titanium-bearing raw materials at trace or minor levels. Despite its low average abundance, its distribution in Fe–Ti–O systems may be strongly heterogeneous at the microscale. Within a single grain, Nb may occur simultaneously as a background isomorphic impurity in Fe–Ti oxide lattices and as localized enrichments associated with TiO_2-rich domains, phase boundaries, or subsolidus transformation products of ilmenite. This heterogeneity is important not only from a mineralogical and crystal-chemical perspective, but also for applied metallurgy, because the speciation of Nb governs the correct interpretation of microanalytical data and affects the pathways of its redistribution during high-temperature processing of titanium-bearing feedstocks.

The physicochemical framework for analyzing such systems is defined by the equilibria of Fe–Ti oxides and their solid solutions. Classical studies of ilmenite–titanomagnetite and ilmenite–hematite assemblages established that phase stability, cation ordering, and component redistribution in the Fe–Ti oxide subsystem are controlled primarily by temperature and oxygen potential (fO_2) [1–5]. Subsequent advances in thermodynamic modeling and computational tools for Fe–Ti–O systems made it possible to relate observed microtextures to phase stability fields and re-equilibration pathways [6–8]. However, these approaches do not in themselves resolve the question of how Nb is actually accommodated in natural Fe–Ti oxide materials or how its crystal-chemical state is linked to the microtextural evolution of the host system.

From a crystal-chemical viewpoint, Nb in ilmenite is commonly regarded as Nb(V) heterovalently substituting for Ti(IV) in octahedral sites, with charge compensation achieved through coupled substitution schemes such as $Fe^{3+} + Nb^{5+} \leftrightarrow 2Ti^{4+}$ and/or $Fe^{2+} + 2Nb^{5+} \leftrightarrow 3Ti^{4+}$ [9–11]. In ordinary ilmenites, this mechanism corresponds to a low background solubility of Nb in the Fe–Ti oxide matrix. At the same time, extensive geochemical evidence demonstrates that TiO_2 phases, particularly rutile, are efficient concentrators of high-field-strength elements, including Nb and Ta, and may accumulate Nb much more effectively than coexisting ilmenite [12–15]. Recent rutile mapping studies also show that Nb-bearing trace-element zoning may be strongly heterogeneous within single grains, reinforcing the need for texture-resolved rather than purely averaged interpretations [16]. Consequently, local Nb enrichments in Fe–Ti oxide assemblages are expected to be related less to uniform enrichment of the ilmenite matrix itself than to the development of TiO_2-rich domains, including rutile lamellae, rims, rutile-like microphases, and products of subsolidus alteration.

This relationship becomes especially important in materials that have undergone staged transformation of ilmenite through ilmenite–pseudorutile–leucoxene sequences, where newly formed TiO_2 phases create additional structural and phase-selective sinks for Nb [17,18]. In practice, this gives rise to a major analytical difficulty: Nb commonly occurs near the detection limit of EDS, so average compositions and even element distribution maps may fail to discriminate reliably between true background Nb dissolved in the lattice and narrow texture-controlled microdomains of Nb enrichment. Under the applied SEM-EDS conditions, the practical detectability of Nb in the matrix should be regarded as being on the order of trace-to-low hundredths of a wt.%, depending on local matrix composition, counting statistics, lamella geometry, and signal overlap. Recent EPMA work on trace-level Nb in rutile further shows that robust low-level Nb quantification requires highly optimized analytical conditions and should not be assumed under routine microanalytical settings [19]. This creates the risk of two opposite interpretative errors. Local maxima may be overinterpreted as evidence for "Nb-rich ilmenite", whereas weak or absent signals may lead to an overly rigid conclusion that Nb-bearing phases are absent. For Fe–Ti oxide

systems, the more appropriate principle is that "not detected" does not mean "absent", and interpretation should be based on local microanalysis, textural context, and comparison of several independent analytical methods [20].

Although a substantial body of literature exists on Fe–Ti oxide thermodynamics, rutile geochemistry, and Nb crystal chemistry, an important gap remains between three levels of description: (i) crystal-chemical mechanisms of Nb incorporation into Fe–Ti oxide structures, (ii) thermodynamic constraints on phase stability in the Fe–Ti–O system, and (iii) the actual microanalytical pattern of Nb distribution in natural and model materials. In other words, previous studies have commonly focused either on Fe–Ti oxide equilibria or on local analytical observations, but much less frequently on an integrated mechanistic framework linking isomorphic substitution, development of TiO_2-rich microdomains, and subsequent segregation of discrete Nb-bearing phases. Recent spectroscopic work further emphasizes that Nb may occupy structurally complex and compositionally variable oxide environments, which complicates straightforward phase-level interpretation in fine-grained ore materials [21].

This unresolved problem defines the rationale of the present study. We test the hypothesis that Nb distribution in the Fe–Ti–O system is fundamentally two-mode in character and should be considered as a sequence of related states: background isomorphic incorporation in the Fe–Ti oxide matrix, Nb-enriched rutile-like domains or ilmenorutile-type solid solutions, and finally segregation into distinct Nb-bearing oxides or niobates. Such an approach does not merely describe the occurrence of Nb in different phases; it aims to explain its redistribution as a function of textural evolution, temperature, and redox conditions.

The study integrates three complementary lines of evidence. First, Nb localization is investigated in a natural ilmenite concentrate by SEM-EDS and WDS mapping with emphasis on textural control. Second, Nb-bearing phases are examined in model TiO_2–FeO–Nb_2O_5 and TiO_2–Fe_2O_3–Nb_2O_5 systems by X-ray diffraction and thermal analysis. Third, thermodynamic modeling is used to constrain phase stability and possible redistribution pathways of Nb in oxide systems. This design makes it possible to follow the same process across different scales, from microdomains in natural grains to phase-stable Nb hosts in model materials.

The aim of this work is to determine the speciation, localization, and redistribution mechanisms of Nb in the Fe–Ti–O system and to propose a mechanistic model linking isomorphic incorporation of Nb in Fe–Ti oxide matrices with its microphase enrichment in the TiO_2 subsystem. The specific objectives are to: (1) substantiate the crystal-chemical mechanisms responsible for background Nb incorporation in ilmenite; (2) identify and semi-quantitatively characterize texture-controlled zones of Nb microphase enrichment; (3) correlate natural microtextures with the phase evolution of Nb hosts in model systems; and (4) define the thermodynamic constraints governing the stability of different forms of Nb occurrence in Fe–Ti–O materials.

The novelty of the study lies in three principal aspects. First, Nb is interpreted as an element showing a two-mode distribution pattern in Fe–Ti–O systems, namely background isomorphic incorporation in Fe–Ti oxide matrices combined with localized microphase enrichment in TiO_2-rich domains. Second, the TiO_2 subsystem is interpreted as the principal concentrator of Nb in the investigated materials, whereas the transition from background distribution to local maxima is controlled not only by bulk composition but also by textural evolution. Third, by combining observations from natural and model materials, the study proposes a coherent mechanistic framework of Nb speciation: isomorphic substitution → microphase enrichment → segregation into Nb-bearing oxides/niobates. In

addition, the study includes a first-order empirical area-based estimate of the contribution of rutile lamellae to the detected Nb budget in representative analyzed grains.

2. Materials and Methods

2.1. Study Objects and Experimental Design

The study was designed to determine the speciation, localization, and redistribution mechanisms of niobium in the Fe–Ti–O/TiO_2 system by combining electron probe microanalysis, X-ray diffraction, thermal analysis, and thermodynamic modeling. The experimental strategy followed a cross-scale approach, from direct identification of Nb-bearing microdomains in a natural Fe–Ti oxide object to phase verification in model oxide systems and subsequent physicochemical interpretation by equilibrium calculations.

Two groups of materials were investigated. The first group consisted of a natural Fe–Ti oxide object represented by an ilmenite concentrate from the Satpaev deposit (Figure 1), which was used to localize Nb and evaluate its distribution between background matrix occurrence and rutile-related local enrichment in the ilmenite matrix–rutile lamellae system. The second group consisted of model TiO_2–FeO–Nb_2O_5 and TiO_2–Fe_2O_3–Nb_2O_5 systems synthesized under controlled thermal conditions and used for phase verification of Nb-bearing hosts and evaluation of their thermal stability. Thermodynamic calculations were additionally applied to interpret phase stability and probable redistribution pathways of Nb in the Fe–Ti–O system [6–8]. The investigated materials, model series, analytical objectives, and methods applied in this study are summarized in Table 1.

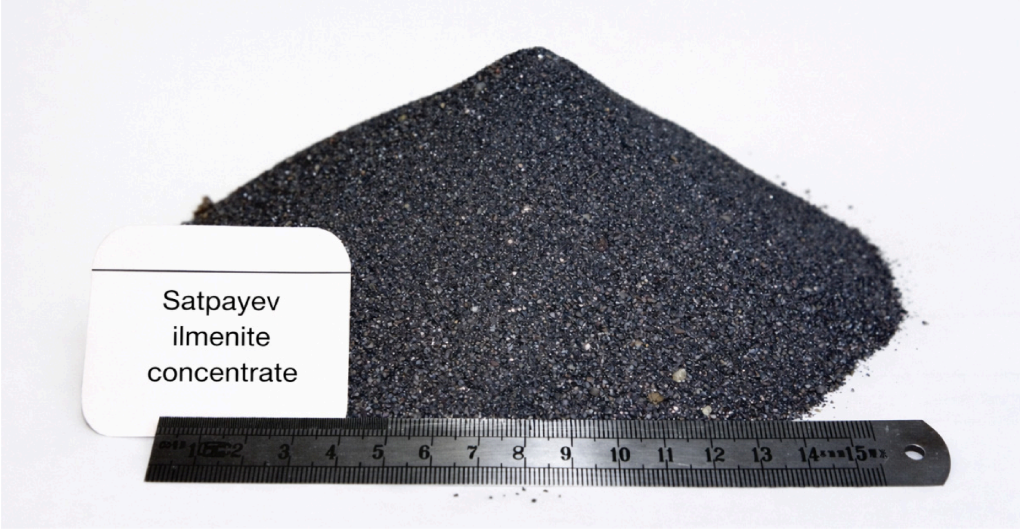


Figure 1. General view of the investigated ilmenite concentrate from the Satpaev deposit.

Table 1. Investigated materials, model sample series, synthesis conditions, analytical objectives, and methods applied in this study.

No.	Object/Series	Composition/Type	Preparation Conditions	Objective	Methods
1	Ilmenite concentrate from the Satpaev deposit	Natural Fe–Ti oxide material	No synthesis	Nb localization; matrix/lamellae distribution	SEM-EDS, WDS, BSE, XRD, HSC
2	FeO series	TiO_2–FeO–Nb_2O_5 (10 g/10 g/1.7 g)	900–1200 °C, 120 min, vacuum	Identification of Nb-bearing hosts in a reducing system	XRD, TG/DTG/DTA, HSC

Table 1. *Cont.*

No.	Object/Series	Composition/Type	Preparation Conditions	Objective	Methods
3	Fe_2O_3 series	TiO_2–Fe_2O_3–Nb_2O_5 (10 g/10 g/1.7 g)	900–1200 °C, 240 min, vacuum	Identification of Nb-bearing hosts in an oxidizing system	XRD, TG/DTG/DTA, HSC
4	Synthesis products	Powders obtained after synthesis	Cooling and grinding	Phase composition and thermal stability	XRD, TG/DTG/DTA
5	Calculated microdomains	Matrix, lamellae, and Nb-rich domains	Derived from SEM-EDS/WDS data	Comparison with equilibrium phase assemblages	HSC Chemistry 6

2.2. Preparation of Model Samples

Two model mixtures were prepared to reproduce Nb-bearing Fe–Ti oxide systems: TiO_2 + FeO + Nb_2O_5 (Figure 2a) and TiO_2 + Fe_2O_3 + Nb_2O_5 (Figure 2b). In both series, the component ratio was 10 g TiO_2:10 g FeO (or Fe_2O_3):1.7 g Nb_2O_5. The starting materials were thoroughly homogenized in an MM400 RETSCH vibration ball mill before heat treatment (Figure 3a).

For the TiO_2–FeO–Nb_2O_5 system, synthesis was carried out at 900, 1000, 1100, and 1200 °C with a holding time of 120 min. For the TiO_2–Fe_2O_3–Nb_2O_5 system, the same temperatures were used, but the holding time was 240 min. Thermal treatment was performed in an SNOL 7.2/1300 vacuum furnace (Figure 3b) at approximately −0.06 MPa. After synthesis, the samples were cooled, removed from the furnace, labeled, and ground into powder for subsequent XRD and thermal analysis.

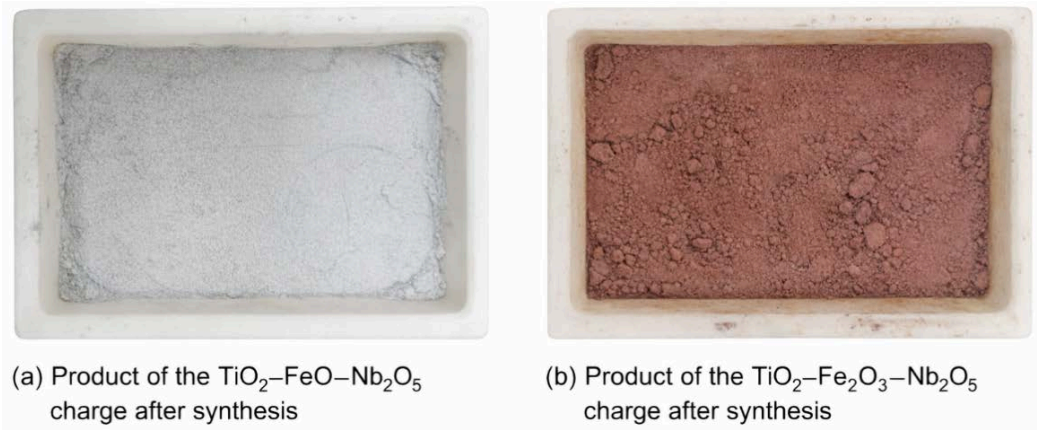


Figure 2. General view of the synthesized products of the TiO_2–FeO–Nb_2O_5 and TiO_2–Fe_2O_3–Nb_2O_5 model series after thermal treatment.

2.3. Sample Preparation for Electron Probe Microanalysis

For SEM-EDS/WDS analysis, powder particles and individual grains, typically in the tens-to-hundreds of micrometers size range, were mounted on brass holders using carbon double-sided conductive tape (NISSIN). This preparation mode allowed the analysis of individual grains and grain sections in backscattered-electron mode and permitted point analysis, EDS mapping, and WDS mapping without resin embedding. The same mounting and orientation procedure was used for all analyzed grains (Figure 4).

For the quantitative evaluation of the first-order Nb partitioning estimate between the matrix and rutile lamellae, only grains showing clearly distinguishable rutile lamellae

or rutile-like domains in BSE images, at least one Nb-bearing domain confirmed by point analysis, and no preparation defects affecting segmentation were considered suitable for interpretation. These selection criteria were applied consistently to the analyzed subset used for the area-based reconstruction.



Figure 3. Equipment used for homogenization and thermal treatment of the model mixtures: (**a**) MM400 RETSCH vibration ball mill; (**b**) SNOL 7.2/1300 vacuum furnace.

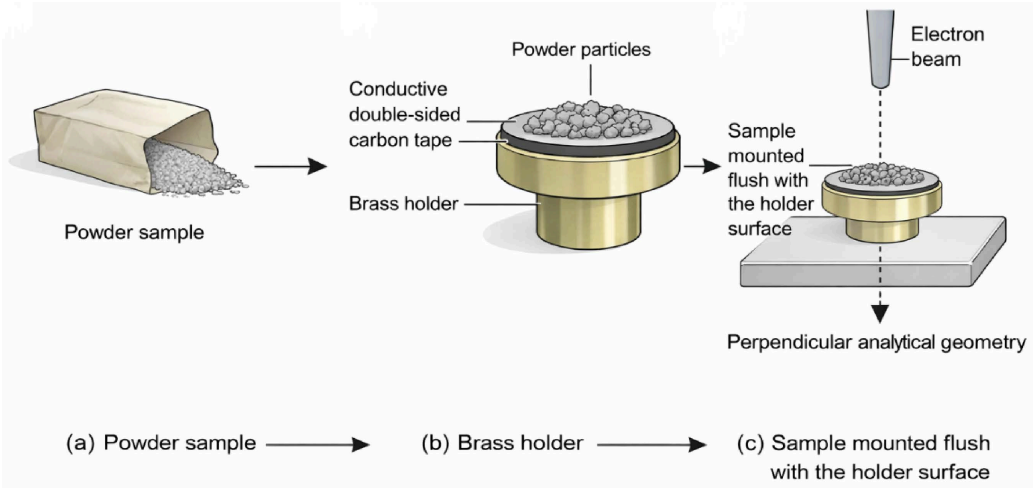


Figure 4. Sample preparation scheme for SEM/EPMA analysis showing particle mounting on a brass holder with carbon double-sided conductive tape and the resulting analytical geometry.

2.4. Electron Probe Microanalysis

Microanalytical measurements were performed on a JEOL JXA-8230 electron probe microanalyzer, JEOL Ltd., Tokyo, Japan, operated in BSE-COMPO mode at an accelerating voltage of 20 kV. EDS analyses were carried out using a Bruker QUANTAX 200 system, Bruker Nano GmbH, Berlin, Germany, equipped with a 60 mm^2 SDD detector. Quantitative data reduction was performed using ZAF correction. Natural minerals analyzed under the same instrumental conditions were used as standards. In total, 78 point analyses, 9 EDS maps, and 3 WDS maps were acquired. The electron beam diameter was 1–2 µm, and the probe current varied between 25 pA and 5 nA depending on the analytical mode and task (Figure 5).



Figure 5. Analytical equipment used in this study: (**a**) JEOL JXA-8230 electron probe microanalyzer; (**b**) Rigaku MiniFlex diffractometer, Rigaku Corporation, Tokyo, Japan; (**c**) STA 409 PC/PG (NETZSCH) simultaneous thermal analyzer, NETZSCH-Gerätebau GmbH, Selb, Germany.

The available WDS data were used primarily as supporting qualitative and semi-quantitative evidence for the presence of Nb-bearing microdomains and for cross-checking the EDS-based localization pattern. Because detailed acquisition parameters were not consistently recorded for all WDS maps, and because the WDS dataset was not systematic enough for full quantitative treatment, these data are interpreted conservatively and are not used as the basis for a rigorous quantitative reconstruction of Nb distribution. Accordingly, the principal analytical basis of the present microdomain-scale interpretation remains SEM-EDS supported by BSE imaging, whereas WDS is used only as an auxiliary line of evidence. The operating conditions, imaging modes, and analytical parameters used in this study are summarized in Table 2.

Table 2. Operating conditions, imaging modes, and analytical parameters of the SEM-EDS/WDS measurements used in this study.

No.	Parameter	Condition/Value	Comment
1	Instrument	JXA-8230 (JEOL)	Electron probe microanalyzer
2	Sample type	Powder samples	Packaged in labeled paper envelopes
3	Sample mounting	Brass holders with carbon double-sided conductive tape (NISSIN)	Mounted flush with the holder cross-section
4	Accelerating voltage	20 kV	Used for imaging and microanalysis
5	Beam current	25 pA–5 nA	Adjusted depending on the analytical task
6	Dead time	Up to 20%	Reported acquisition condition
7	Imaging modes	BSE-COMPO; SEI	BSE-COMPO used as the principal imaging mode for documented interpretation
8	Magnification range	×40–×4000	Used for observation of structures from submicron to hundreds of micrometers

Table 2. *Cont.*

No.	Parameter	Condition/Value	Comment
9	Number of documented micrographs	28	Used for microstructural documentation
10	Point analyses (documented)	78	SEM-EDS point microanalyses
11	Selected-area EDS analyses	3	EDS analyses acquired from selected areas
12	EDS elemental maps	9	Documented EDS mappings
13	WDS elemental maps	3	Documented WDS mappings
14	WDS point analyses	2	Additional WDS point measurements
15	Additional undocumented point analyses	>300	Used for verification of structural representativeness
16	Quantification procedure	Semi-quantitative EPMA with automatic ZAF correction	Built-in software
17	Main reported image metadata	Magnification, scale marker (μm), date, time, imaging mode	Included on SEM micrographs

Note: BSE-COMPO was used as the principal imaging mode for interpretation because it provided more informative compositional contrast than SEI imaging. Quantitative values were obtained on a semi-quantitative basis using built-in EPMA software with automatic ZAF correction. Within this analytical framework, WDS observations were treated only as supporting qualitative/semi-quantitative evidence and were not used for full quantitative reconstruction of Nb distribution.

2.5. X-Ray Diffraction Analysis

Phase compositions of the synthesized samples were determined by X-ray diffraction using a Rigaku MiniFlex diffractometer in θ–2θ geometry. Data were collected over the 2θ range 10–90° with a step size of 0.02° and a scan speed of 2°/min. Phase identification was performed using the PDF-2 ICDD database (Release 2022) and HighScore Plus software SmartLab Studio II x64, version 4.6.864.0. The relative contents of the major phases were estimated on a semi-quantitative basis; no Rietveld refinement was performed. Possible minor phases represented only by very weak reflections or by poorly crystalline components were interpreted cautiously. In the present work, XRD was used for phase identification rather than direct elemental Nb determination; accordingly, the practical detectability of minor Nb-bearing phases depends on their abundance, crystallinity, and peak overlap, and is typically limited to several wt.% for well-crystallized minor phases. Therefore, phase assignments involving weak reflections were treated as tentative or semi-quantitative where appropriate.

2.6. Thermal Analysis

Thermal effects and mass changes in the synthesized products were evaluated using an STA 409 PC/PG (NETZSCH) simultaneous thermal analyzer by TG/DTG/DTA in the temperature range 20–1000 °C at a heating rate of 10 °C/min in a nitrogen atmosphere. For each sample, the residual mass, characteristic peak positions, and temperature intervals of thermal effects were recorded and compared between the FeO- and Fe2O3-based model systems. The thermal analysis data were used primarily to compare relative stability and transformation behavior between the synthesized phase assemblages rather than for stand-alone phase identification.

2.7. Thermodynamic Modeling

Thermodynamic interpretation was carried out using HSC Chemistry 6. In the Reaction Equations module, temperature dependences of ΔG(T) were calculated for key reactions related to the formation and transformation of Nb-bearing compounds in the oxide systems under consideration. Stability fields of phases were visualized using T_{pp} and L_{pp} diagrams for the Fe–Ti–O, Nb–C–O, and Nb–Fe–O subsystems. Equilibrium phase compositions for local microdomains were estimated using HSC Mineralogy/Mineralogy Iterations. The input data were oxide compositions normalized to 100 wt.% and derived from SEM-EDS/WDS analyses [6–8]. In the present work, these calculations were used to constrain thermodynamically plausible phase relations and redistribution pathways, rather than as direct experimental proof of phase identity in the investigated materials.

The thermodynamic calculations included: (i) reduction of Fe–Ti oxides and formation of Ti-bearing phases in the $FeTiO_3$–C system at 900–1700 °C; (ii) phase-stability relations in the Fe–Ti–O subsystem; (iii) carbide formation in the Nb_2O_5–C system at 900–1700 °C; (iv) stability of Nb carbides and $NbFe_2$ in the Nb–C–O and Nb–Fe–O systems at 900–2000 °C; (v) equilibrium phase calculations for local SEM-EDS/WDS-derived microcompositions at 700–1700 °C; and (vi) evaluation of the effects of minor components such as Mg, Mn, Al, and Si on the oxide phase assemblage. Accordingly, the thermodynamic results were interpreted as equilibrium-based physicochemical constraints to be compared with the microanalytical, diffraction, and thermal datasets, rather than as a stand-alone basis for definitive phase assignment. The thermodynamic calculations performed in this study are summarized in Table 3.

Table 3. Thermodynamic calculations performed for interpretation of Nb behavior in the Fe–Ti–O/TiO_2 system.

No.	HSC Module	System	Temperature Range (°C)	Objective
1	Reaction Equations	$FeTiO_3$–C	900–1700	Reduction of Fe–Ti oxides and formation of Ti-bearing phases
2	T_{pp}/L_{pp} Diagrams	Fe–Ti–O	—	Phase-stability fields of Fe–Ti oxide assemblages
3	Reaction Equations	Nb_2O_5–C	900–1700	Carbide formation and stability of NbC/Nb_2C
4	T_{pp}/L_{pp} Diagrams	Nb–C–O; Nb–Fe–O	900–2000	Stability of Nb carbides and the $NbFe_2$ intermetallic
5	Mineralogy Iterations	Local SEM-EDS/WDS-derived compositions	700–1700	Equilibrium phase calculation from normalized oxide compositions
6	Reaction Equations/T_{pp}	Fe–Ti–O with minor components	900–1700	Evaluation of the effects of Mg, Mn, Al, Si, and other minor elements on phase assemblages

2.8. Evaluation of Two-Mode Nb Localization

For the natural Fe–Ti oxide grains, Nb localization was considered in terms of a two-mode model: (1) background isomorphic incorporation in the ilmenite matrix and (2) local Nb enrichments in rutile lamellae or rutile-like microphases. The existence of this dual distribution was evaluated using combined BSE imaging, point analysis, and element mapping. On the basis of the analyzed subset of representative grains, a first-order area-based estimate suggested that approximately 60–80% of the detected Nb was associated with the lamellar channel.

The contribution of the lamellar channel was estimated using a first-order two-dimensional area-based approach. For each suitable grain, two categories of regions were distinguished: L, corresponding to rutile lamellae or other Nb-enriched rutile-like domains, and M, corresponding to the surrounding ilmenite matrix. Segmentation of the L and M domains was performed on representative BSE micrographs using a two-class image-analysis workflow, in which lamellar regions and the surrounding matrix were delineated on the basis of compositional contrast and morphological continuity. Assignment of domains to the L category was supported by elevated Nb contents in point analyses and/or distribution maps. Only grains showing a clear lamella–matrix contrast and at least one Nb-enriched lamellar or rutile-like domain confirmed by point EDS analysis were included in the calculation. The 60–80% interval reported in this study represents the range obtained for the analyzed subset of representative grains and should be interpreted as a first-order empirical estimate derived from two-dimensional image segmentation combined with local semi-quantitative EDS data, rather than as a rigorous stereological determination of the full three-dimensional Nb budget. No formal propagated uncertainty was calculated for this estimate; accordingly, the reported range reflects the observed variation in lamellar area fraction and local Nb concentrations between the analyzed grains.

The fraction of Nb associated with the lamellar channel was calculated as follows:

$$S_{Nb}^{L} = \frac{A_L \cdot \overline{C_{Nb}^{L}}}{A_L \cdot \overline{C_{Nb}^{L}} + A_M \cdot \overline{C_{Nb}^{M}}} \quad (1)$$

where

- S_{Nb}^{L} is the fraction of the total detected Nb associated with the lamellar channel;
- A_L and A_M are the area fractions of the lamellar and matrix domains, respectively;
- C_{Nb}^{L} and C_{Nb}^{M} are the average Nb concentrations in the lamellar and matrix domains, respectively.

The complementary fraction of Nb associated with the matrix was calculated as:

$$S_{Nb}^{M} = \frac{A_M \cdot \overline{C_{Nb}^{M}}}{A_L \cdot \overline{C_{Nb}^{L}} + A_M \cdot \overline{C_{Nb}^{M}}} = 1 - S_{Nb}^{L} \quad (2)$$

The overall computational workflow used to link the SEM-EDS/WDS data with HSC Mineralogy calculations and the interpretation of Nb partitioning is summarized in Figure 6.

2.9. Interpretation Principles and Methodological Limitations

Interpretation of the analytical results was performed with explicit consideration of methodological limitations. In particular, the absence of a confident EDS signal for Nb was not taken to mean the absence of Nb from the analyzed area. Low and near-zero Nb values, especially in the matrix, were assessed with regard to matrix effects, lamella geometry, spatial resolution, and possible overlap of signals between lamellae and the surrounding

matrix; accordingly, such values were interpreted conservatively as being consistent with trace background incorporation rather than as a standalone rigorous quantitative proof. Bulk analytical methods such as ICP-OES or XRF were not used in the present work because the aim was not bulk Nb determination, but microdomain-scale localization and comparison of matrix and lamellar Nb occurrence. Such methods may be useful for bulk chemical control, but they do not resolve the micron-scale textural partitioning addressed here. Likewise, phases tentatively assigned from isolated or very weak XRD reflections were treated cautiously as possible minor crystalline constituents rather than unequivocally confirmed major constituents, and all phase identifications remained semi-quantitative in nature because no Rietveld refinement was performed.

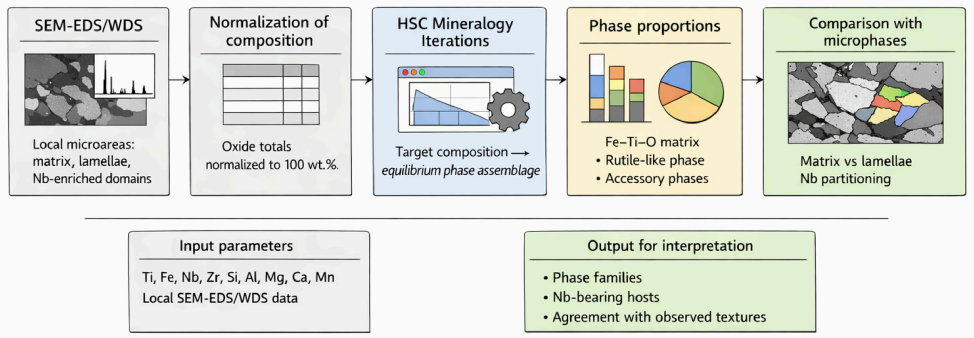


Figure 6. Computational workflow used for linking SEM-EDS/WDS data with HSC Mineralogy calculations and comparison of calculated phase assemblages with observed microdomains.

Accordingly, the microanalytical, diffraction, thermal, and thermodynamic datasets were interpreted in combination rather than as mutually independent stand-alone proof of any single Nb-host assignment [18].

3. Results

3.1. Natural Fe–Ti Oxide Material: Ilmenite Concentrate from the Satpaev Deposit

3.1.1. Element Distribution Maps and Background Nb Signal

EDS mapping of the natural Fe–Ti oxide material shows that Ti and Fe form the main Fe–Ti oxide matrix, whereas Zr is concentrated in discrete grains, most likely zircon or zircon-related phases. In contrast, Nb is detected at a generally low level over the mapped field and appears mainly as a weak background signal with only occasional local enrichments. This pattern is consistent with two analytical features of the material: first, a substantial fraction of Nb occurs at trace concentrations close to the detection limit of SEM-EDS under the applied conditions; second, local Nb-rich domains are small enough to be partly averaged out in integrated map-based observations. A similar contrast between weak integrated Nb signals and localized Nb enrichment has been reported for Fe–Ti oxide systems in the literature [22,23], and a representative mapped field illustrating this distribution pattern is shown in Figure 7.

To provide a quantitative background estimate, the mean composition of the mapped area was calculated. The resulting average composition is presented in Table 4. The absolute Nb content in the integrated map is low (0.04 wt.%), and this value should be interpreted only as integrated evidence that Nb is present somewhere within the analyzed field of view, even where no strong discrete enrichments are visually expressed in the map average. At the same time, this mapped-field value should be interpreted as integrated evidence that Nb is present within the analyzed field of view, rather than as a rigorous standalone quantification of matrix Nb, because local Nb-enriched microdomains may be partly averaged into the mapped-field mean and matrix-level Nb occurs near the practical

interpretative limit of SEM-EDS. Accordingly, the mapped-field Nb value is treated here as compatible with low-level background Nb occurrence in the analyzed Fe–Ti oxide material, but not as direct quantitative proof of uniform matrix incorporation.

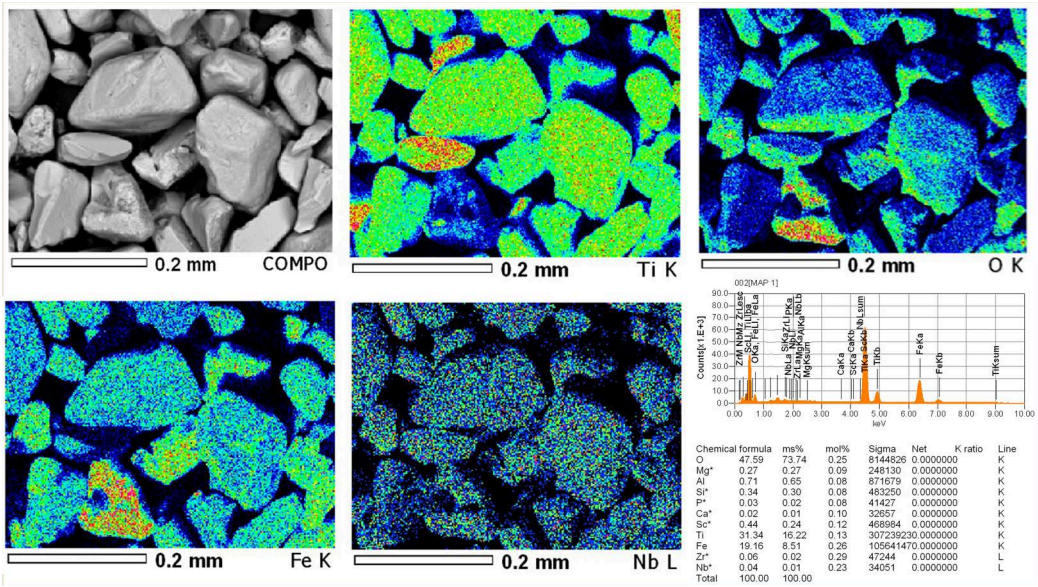


Figure 7. Representative EDS elemental distribution map of an Fe–Ti oxide grain showing the distributions of Ti, Fe, O, and Nb.

Table 4. Average chemical composition of the mapped area determined from EDS data.

Component	O	Ti	Fe	Nb	Zr	Al	Si	Mg	Cr	Ca	P	Sc
wt.%	47.59	31.34	19.16	0.04	0.06	0.71	0.34	0.27	—	0.02	0.03	0.44

Note. The Nb and Zr contents in the mapped field represent integrated averages and should not be interpreted as spatially uniform concentrations. In particular, the mapped-field Nb value does not exclude the presence of localized Nb-enriched domains revealed by point analysis and higher-magnification observations.

3.1.2. Nb-Enriched Rutile Lamellae at Higher Magnification

At higher magnification in BSE mode, a morphologically distinct rutile-like component is clearly observed in the form of thin lamellae or narrow inclusions. In these domains, Nb reaches approximately 0.7–1.0 wt.%, whereas in the surrounding ilmenite matrix Nb remains at trace levels and commonly does not exceed 0.05 wt.% under the same analytical conditions. The compositional contrast between lamellae and matrix therefore becomes much clearer at the local scale than in integrated maps.

Point EDS analyses performed on characteristic Nb-enriched areas are consistent with this local enrichment. The measured Nb contents in the representative points range from 0.76 to 0.98 wt.%, indicating a stable order of magnitude for the Nb-rich lamellar component; representative point spectra and analyses for these Nb-enriched domains are shown in Figure 8. The corresponding quantitative point analyses are summarized in Table 5. In the studied natural material, Nb is not interpreted as occurring predominantly as free individual Nb particles. Instead, it is inferred to be mainly oxide-bound: at background levels as a trace oxide-bound component interpreted as consistent with low-level isomorphic incorporation in Fe–Ti oxide lattices, and locally as enrichment within rutile-like lamellae or rutile-related oxide microdomains. Accordingly, the relevant morphological scale is that of the lamellar or rutile-like host domain rather than that of a separate Nb particle.

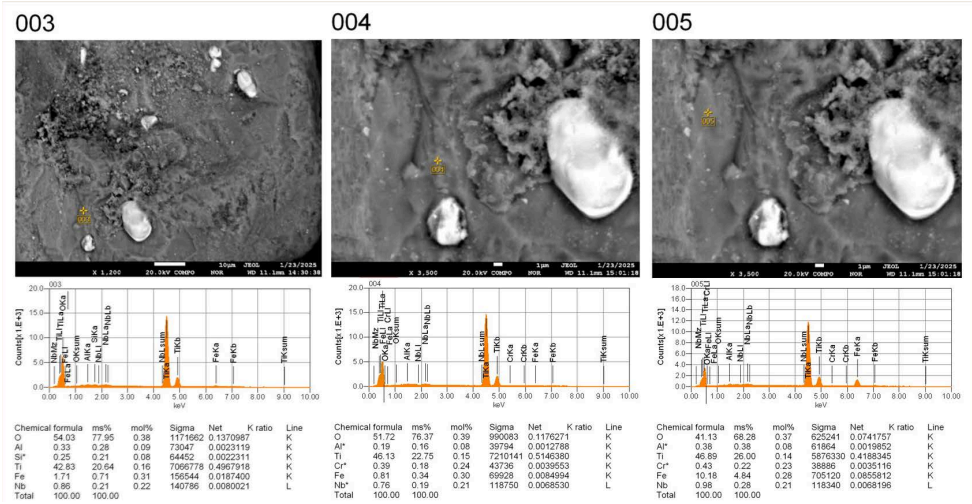


Figure 8. Representative point EDS spectra and quantitative analyses for locally Nb-enriched domains.

Table 5. Representative point EDS analyses of Nb-enriched domains.

Point	O	Ti	Fe	Nb	Al	Si	Cr
003	54.03	42.83	1.71	0.86	0.33	0.25	—
004	51.72	46.13	0.81	0.76	0.19	—	0.39
005	41.13	46.89	10.18	0.98	0.38	—	0.43

The Fe content of the Nb-enriched domains varies noticeably, especially in point 005, which suggests either signal overlap between thin lamellae and the underlying matrix or the presence of transitional microdomains between the rutile-like component and the Fe–Ti oxide host. In the present work, "transitional microdomains" refers to narrow boundary or mixed-signal zones in which the analyzed volume likely includes both the rutile-like lamella and adjacent Fe–Ti oxide material, and/or zones of incomplete local separation between the two components. For this reason, the observed domains are more appropriately described as Nb-enriched rutile-like microdomains rather than unequivocally as pure rutile [12,13,24,25].

3.1.3. First-Order Estimate of Nb Distribution Between Lamellae and Matrix

The qualitative observation of two-mode Nb localization was further translated into a first-order empirical area-based estimate using the approach described in Section 2.8. The fraction of Nb associated with the lamellar channel was calculated according to Equation (1), whereas the complementary matrix contribution was defined by Equation (2). In this approximation, rutile lamellae or rutile-like Nb-enriched domains were treated as one component and the surrounding ilmenite matrix as the second component. The estimated contribution of the lamellar channel depends on the area fraction of lamellae and on the contrast between Nb concentrations in the lamellae and in the matrix.

Under representative conditions, the area fraction of lamellae is about 0.08–0.18, Nb in lamellae is approximately 0.70–1.00 wt.%, and Nb in the matrix is approximately 0.02–0.05 wt.%. In this interpretation, matrix Nb is interpreted as a trace oxide-bound background component compatible with low-level isomorphic incorporation, whereas lamellar Nb corresponds to local enrichment in rutile-like oxide domains rather than to discrete metallic or free Nb particles. Because the Nb concentration in the lamellae exceeds that of the matrix by more than an order of magnitude, even a relatively small area fraction of lamellae may account for a substantial share of the detected Nb budget within representative analyzed sections. The corresponding first-order estimate is summarized in Table 6.

Table 6. First-order estimate of Nb distribution between rutile lamellae and the ilmenite matrix.

Parameter	Lower Estimate	Upper Estimate
Area fraction of lamellae, A_L	0.08	0.18
Nb in lamellae, $\overline{C_{Nb}^{L}}$ (wt.%)	0.70	1.00
Nb in matrix, $\overline{C_{Nb}^{M}}$ (wt.%)	0.05	0.02
Estimated fraction of Nb in lamellar channel, S_{Nb}^{L}	~0.60	~0.80

Note: The values shown in Table 6 represent a first-order 2D area-based estimate derived from representative analyzed grains and local semi-quantitative EDS data. They should not be interpreted as a rigorous stereological reconstruction of the full three-dimensional Nb budget.

These first-order estimates suggest that approximately 60–80% of the detected Nb in representative analyzed grains and sections is associated with rutile lamellae or rutile-like domains, whereas the remaining fraction is retained in the matrix at trace background levels interpreted as consistent with low-level isomorphic incorporation. Because the estimate is derived from two-dimensional sections, semi-quantitative EDS data, and representative rather than statistically exhaustive grain selection, it should be regarded as a first-order empirical result rather than a rigorous stereological determination or a robust quantitative determination of the full Nb budget [12,26–30]. A representative BSE image illustrating this two-mode localization pattern is shown in Figure 9.

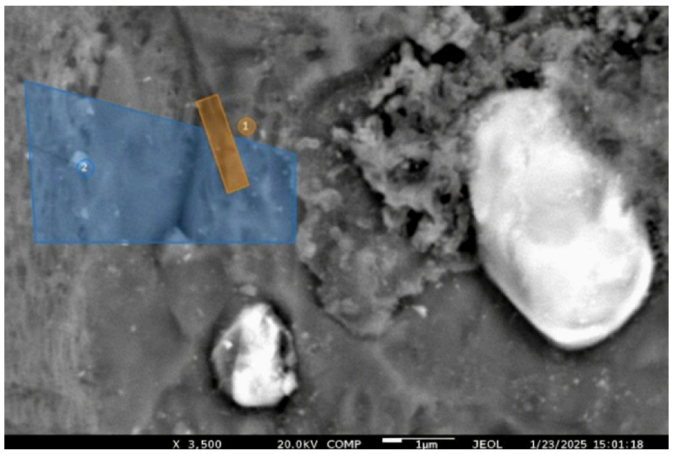


Figure 9. Representative BSE image illustrating the two-mode localization of Nb in an ilmenite grain: (1) trace Nb in the matrix; (2) local Nb enrichment in rutile lamellae.

3.2. Model TiO_2–FeO–Nb_2O_5 and TiO_2–Fe_2O_3–Nb_2O_5 Systems

3.2.1. XRD Identification of Nb-Bearing Phases

X-ray diffraction patterns of the synthesized model samples show that the principal Nb-bearing phase over the investigated temperature range is interpreted on a semi-quantitative XRD basis as an ilmenorutile-like solid solution with the generalized composition (Ti,Fe,Nb)O_2. In both model systems, this phase is already present in the lower part of the investigated interval, i.e., at 900–1000 °C, and remains an important component of the phase assemblage throughout the investigated thermal interval.

At higher temperatures, additional Nb-bearing phases are tentatively assigned in both systems on a semi-quantitative XRD basis. These include $FeNbO_4$, Ti niobates, and complex Fe–Ti–Nb oxides, suggesting that the phase state of Nb evolves from predominantly solid-solution retention toward partial segregation into discrete Nb-bearing compounds as temperature increases. The XRD data also show the simultaneous development of typical Fe–Ti oxide phases, including pseudobrookite Fe_2TiO_5 and Ti-bearing hematite.

These phase relations should be understood as semi-quantitative diffraction-based indications of Nb-host evolution rather than as fully quantitative phase determinations. The corresponding XRD patterns of the synthesized model samples are shown in Figure 10.

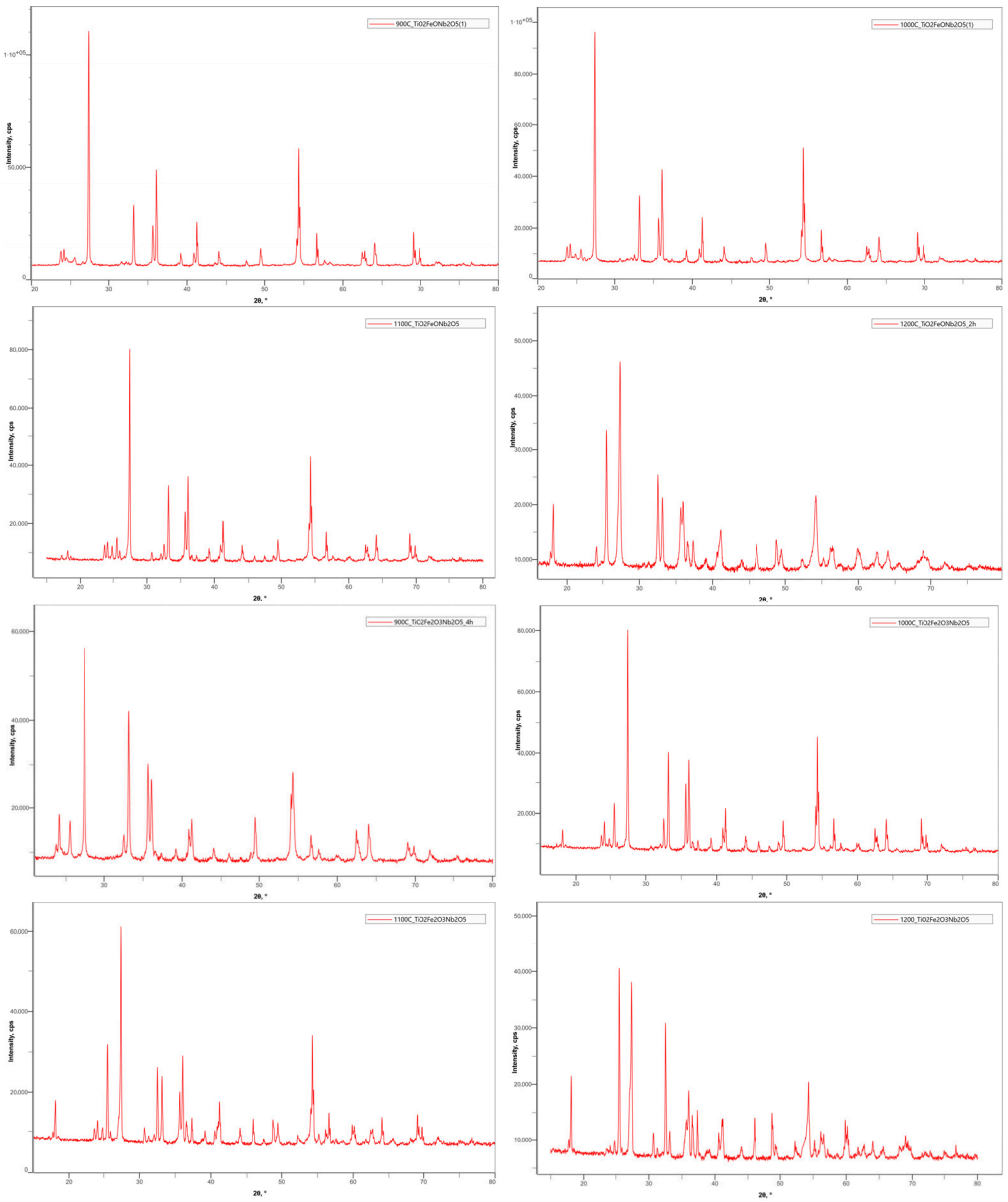


Figure 10. XRD patterns of synthesized model samples in the TiO_2–FeO–Nb_2O_5 and TiO_2–Fe_2O_3–Nb_2O_5 systems.

3.2.2. Semi-Quantitative Phase Composition of the FeO Series

The TiO_2–FeO–Nb_2O_5 series shows a strongly rutile-oriented phase assemblage at 900–1000 °C, where ilmenorutile is the dominant phase. At 900 °C, the ilmenorutile fraction reaches 65.2 wt.%, and at 1000 °C it increases slightly to 66.8 wt.%. Residual Nb_2O_5 is still detectable at these temperatures, suggesting incomplete incorporation of Nb into the dominant oxide host.

At 1100 °C, the phase assemblage becomes more complex, and the ilmenorutile fraction decreases to 37.8 wt.% while TiO2-type oxide reaches 31.5 wt.%. At 1200 °C, the contribution of pseudobrookite increases sharply to 36.5 wt.%, accompanied by Ti-bearing hematite at 15.6 wt.%, whereas ilmenorutile remains significant at 47.9 wt.%.

The FeO-based system therefore suggests, on a semi-quantitative XRD basis, that ilmenorutile is the principal Nb-bearing host at lower temperatures, whereas higher temperatures promote redistribution of Ti and Fe among additional Fe–Ti oxide phases and modify the phase balance of Nb-bearing solids. These trends are interpreted as semi-quantitative phase-evolution patterns rather than as fully quantitative phase-balance determinations.

3.2.3. Semi-Quantitative Phase Composition of the Fe_2O_3 Series

In the TiO_2–Fe_2O_3–Nb_2O_5 series, ilmenorutile is present across the entire temperature range, but the system shows a more systematic increase in pseudobrookite content with increasing temperature. The ilmenorutile fraction decreases gradually from 44.4 wt.% at 900 °C to 38.7 wt.% at 1200 °C, while pseudobrookite rises from 12.5 to 46.6 wt.%.

The Fe_2O_3 series also suggests the appearance of additional Nb-bearing phases in specific temperature windows, including iron niobium oxide, a complex Fe–Ti–Nb oxide, and an iron enneaicosaoxo-hendecaniobate-type phase on a semi-quantitative XRD basis. Residual Nb_2O_5 is observed only at 900 °C, indicating that incorporation and redistribution of Nb become more complete at higher temperatures.

Overall, the Fe_2O_3-based system is characterized by persistent ilmenorutile together with a stronger tendency toward the formation of pseudobrookite and additional Nb-bearing oxides as temperature increases. Taken together, Tables 7 and 8 suggest on a semi-quantitative XRD basis that the ilmenorutile-like phase remains the principal Nb-bearing host in both model systems over a broad interval, reflecting a more advanced stage of redistribution rather than replacement of the principal TiO_2-related Nb host. These phase relations are interpreted on a semi-quantitative XRD basis and should be understood as trends in Nb-host evolution rather than as fully quantitative phase-balance determinations.

Table 7. Semi-quantitative phase composition of the TiO_2–FeO–Nb_2O_5 system determined by XRD.

Phase	900 °C	1000 °C	1100 °C	1200 °C
Hydrohematite	29.7	23.7	26.0	0.0
Ilmenorutile (Fe,Ti,Nb)O_2	65.2	66.8	37.8	47.9
Nb_2O_5	5.8	10.1	0.0	0.0
TiO_2-type oxide	0.0	0.0	31.5	0.0
Ti-bearing hematite	0.0	0.0	0.0	15.6
Pseudobrookite (Fe_2TiO_5)	0.0	0.0	0.0	36.5

Table 8. Semi-quantitative phase composition of the TiO_2–Fe_2O_3–Nb_2O_5 system determined by XRD.

Phase	900 °C	1000 °C	1100 °C	1200 °C
Ilmenorutile (Fe,Ti,Nb)O_2	44.4	47.4	44.5	38.7
Pseudobrookite (Fe_2TiO_5)	12.5	15.4	30.4	46.6
Ti-bearing hematite	38.8	31.5	0.0	6.0
$Fe_{1.696}Ti_{0.228}O_3$	0.0	0.0	21.0	0.0
Iron enneaicosaoxo-hendecaniobate	0.0	5.7	4.1	0.0
Iron(III) titanium(IV) niobium(V) oxide	0.0	0.0	0.0	5.5
Nb_2O_5	4.3	0.0	0.0	0.0
Iron(III) niobium oxide	0.0	0.0	0.0	3.2

3.3. Thermal Analysis of Model Systems

3.3.1. TiO_2–FeO–Nb_2O_5 Series

The thermal behavior of the FeO series shows a marked dependence on synthesis temperature. Samples synthesized at 900 °C display only minor mass loss (−0.29%), with thermal effects observed between 50 and 725 °C. In contrast, the sample synthesized at

1000 °C shows the most pronounced instability, with a mass loss of −8.35% and several peaks between 290 and 812 °C, indicating active decomposition or restructuring processes. In the context of the phase data obtained in this study, this behavior is interpreted as reflecting incomplete stabilization of the Nb-bearing oxide assemblage in the FeO branch, accompanied by ongoing redistribution among ilmenorutile-like, TiO_2-related, and Fe-bearing oxide components. The corresponding thermal characteristics are summarized in Table 9.

The thermal pattern changes substantially in the 1100–1200 °C range. At 1100 °C, the sample shows near-stable behavior, with an apparent mass change of about +0.3% within experimental uncertainty. At 1200 °C, only a moderate mass loss (−1.23%) is observed, suggesting a more stable phase assemblage relative to the 1000 °C sample. These thermal trends are interpreted comparatively, in combination with the XRD results, rather than as stand-alone proof of phase identity. The TG/DTG/DTA curves of the TiO_2–FeO–Nb_2O_5 series are shown in Figure 11.

Table 9. Thermal characteristics of the TiO_2–FeO–Nb_2O_5 series.

Synthesis Temperature	Mass Change (TG)	Characteristic Range (°C)	Main Peaks (°C)	Interpretation
900 °C	−0.29%	50–725	50, 114, 324, 557, 725	Moisture removal; Nb_2O_5 recrystallization; early formation of Nb-bearing solid solution
1000 °C	−8.35%	290–812	290, 327, 387, 564, 784, 812	Pronounced instability; active phase reorganization and incomplete stabilization of the Nb-bearing oxide assemblage
1100 °C	+0.3% (stable)	26–782	47, 83, 129, 324, 606, 782	Completion of diffusional processes; stabilization of Fe–Ti–Nb oxide solid solution
1200 °C	−1.23%	297–742	340, 448, 555, 742	Structural ordering and thermal stabilization of Nb-bearing oxide assemblage

3.3.2. TiO_2–Fe_2O_3–Nb_2O_5 Series

The Fe_2O_3 series shows generally higher thermal stability than the FeO series. Residual masses range from 99.33 to 101.49%, indicating comparatively small overall mass changes. At 900 and 1000 °C, thermal effects are distributed over broad intervals, but the system does not exhibit the pronounced instability observed in the FeO branch at 1000 °C. The corresponding thermal characteristics are summarized in Table 10.

At 1100 and 1200 °C, the Fe_2O_3 series displays multiple thermal events that reflect progressive reorganization and stabilization of the oxide assemblage. The 1200 °C sample exhibits the highest residual mass and the most thermally stable behavior of the entire series. As in the FeO-based system, these thermal effects are interpreted comparatively and in conjunction with the diffraction data, rather than as stand-alone proof of phase identity. The TG/DTG/DTA curves of the TiO_2–Fe_2O_3–Nb_2O_5 series are shown in Figure 12.

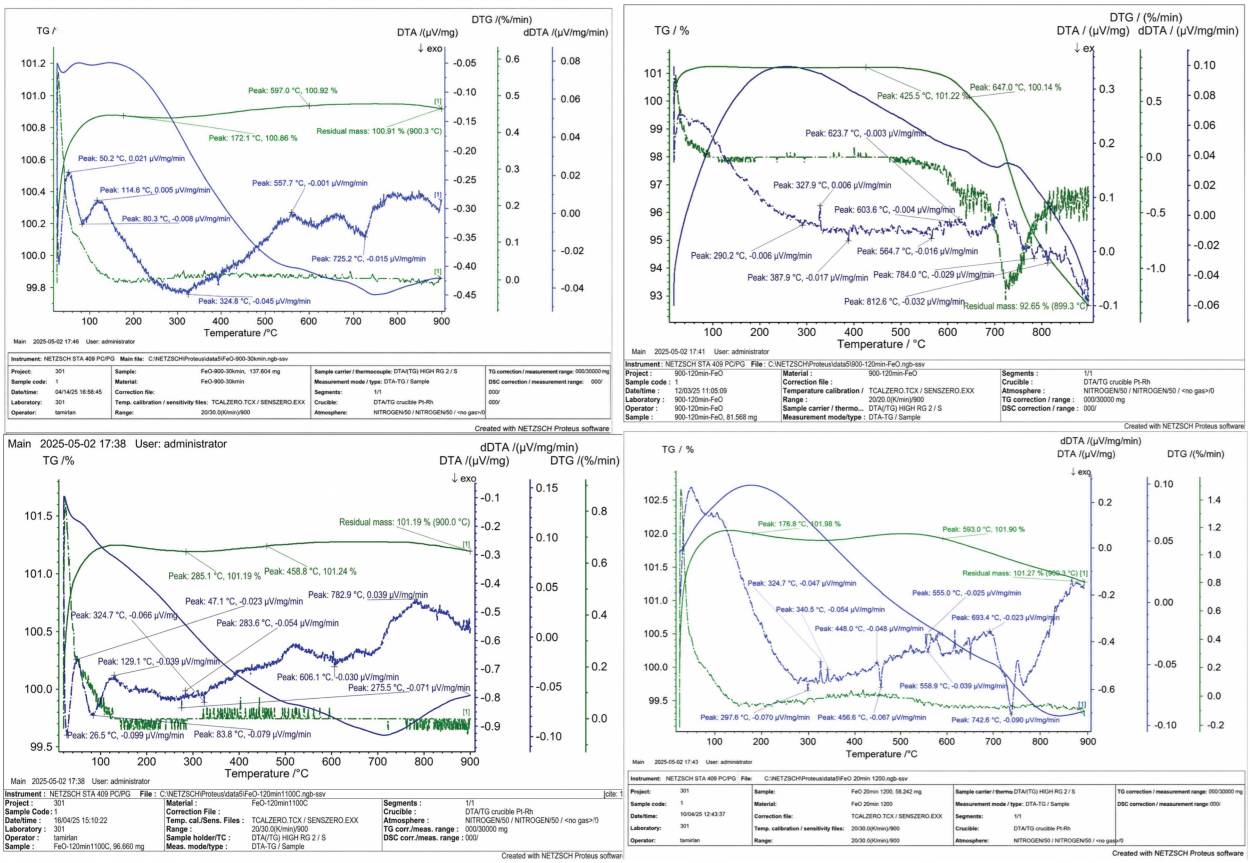


Figure 11. TG/DTG/DTA curves of the TiO_2–FeO–Nb_2O_5 series synthesized at 900, 1000, 1100, and 1200 °C; heating rate 10 °C/min; nitrogen atmosphere.

Table 10. Thermal characteristics of the TiO_2–Fe_2O_3–Nb_2O_5 series.

Synthesis Temperature	Residual Mass (%)	Characteristic Range (°C)	Main Peaks (°C)	Comment
900 °C	99.33	80–675	80.3, 117.1, 277.1, 581.0, 674.5	Partial dehydration and weak ordering effects
1000 °C	100.69	46–741	46.6, 117.8, 258.6, 533.5, 741.7	More pronounced recrystallization; development of Nb-bearing phases
1100 °C	100.31	81–788	81.4, 124.8, 252.2, 449.0, 453.5, 573.9, 659.4, 738.9, 788.8	Active reorganization and multiple endo-/exo-effects
1200 °C	101.49	376–799	376.0, 681.9, 760.0, 763.1, 764.5, 768.1, 799.2	Maximum stabilization and highest thermal resistance

3.3.3. Summary of Thermal Behavior

Taken together, the thermal data indicate that the temperature interval 1100–1200 °C is the most favorable for stabilization of Nb-bearing oxide assemblages in both model systems. The FeO branch is characterized by a pronounced instability around 1000 °C, whereas the Fe_2O_3 branch shows a smoother and more stable thermal evolution over the same interval. These observations are consistent with the XRD results, which show persistent ilmenorutile and progressively more stable Fe–Ti–Nb oxide assemblages at elevated temperatures, although these relations should be interpreted as comparative phase-stability trends rather than as fully quantitative phase determinations.

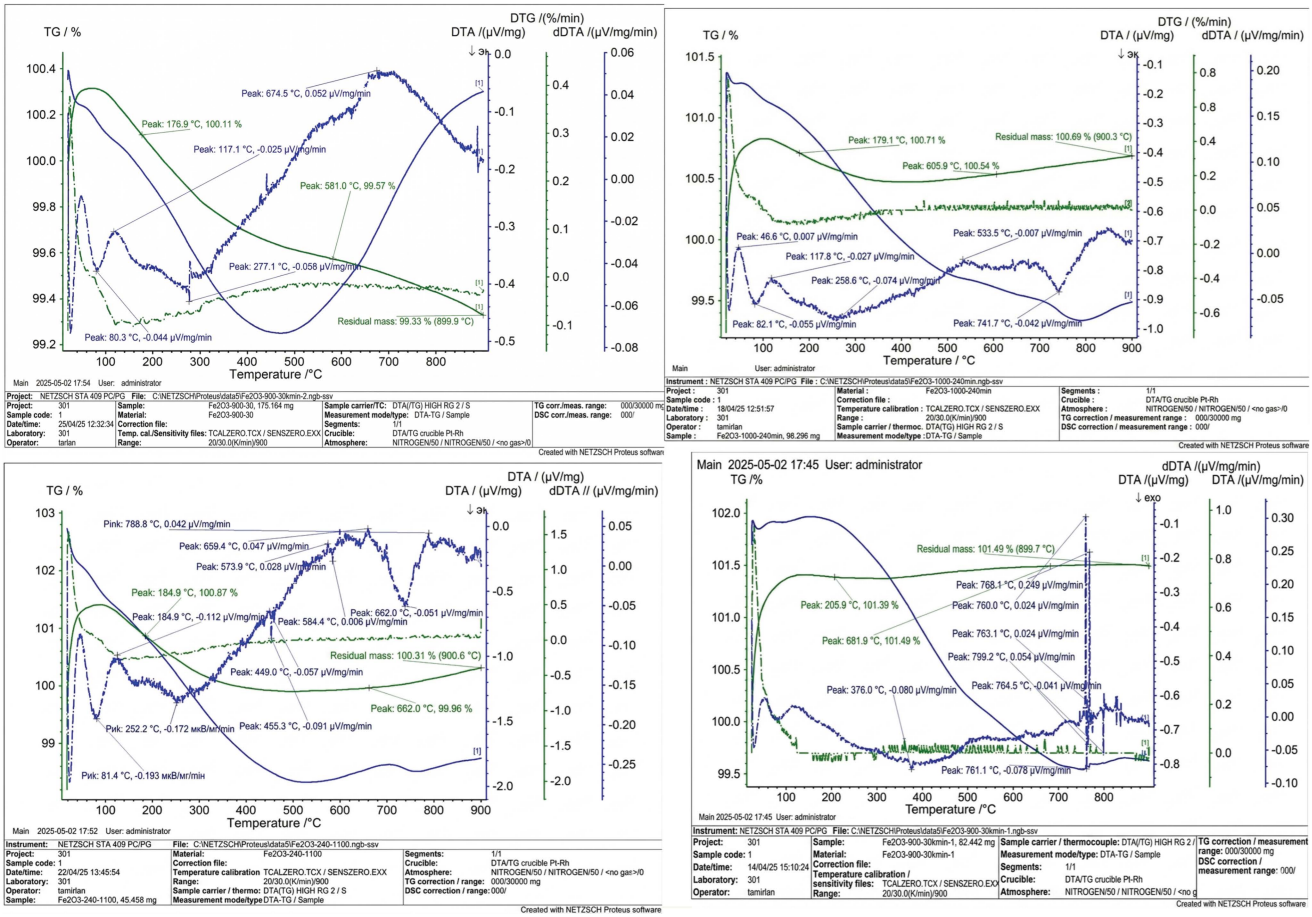


Figure 12. TG/DTG/DTA curves of the TiO_2–Fe_2O_3–Nb_2O_5 series synthesized at 900, 1000, 1100, and 1200 °C; heating rate 10 °C/min; nitrogen atmosphere.

3.4. Thermodynamic Modeling Results

3.4.1. Phase-Stability Relations in the Fe–Ti–O, Nb–O–C, and Nb–O–Fe Systems

The thermodynamic calculations provide a physicochemically grounded framework for interpreting the phase evolution of Nb in the investigated oxide systems. In the Fe–Ti–O subsystem, the predominance and phase-stability diagrams show that TiO_2 and Ti-rich Fe–Ti oxides remain stable over a wide range of temperatures and oxygen potentials, thereby defining the principal oxide framework within which Nb redistribution takes place. These calculations are consistent with the experimental observation that TiO_2-related phases and Fe–Ti oxide assemblages dominate both the natural material and the synthesized systems.

In the Nb–O–C subsystem, the calculations indicate that decreasing oxygen potential and increasing temperature progressively shift Nb from higher oxides toward lower oxides, metallic Nb, and finally carbide-bearing fields. In particular, the stability domains of NbC and Nb_2C expand under strongly reducing conditions, whereas Nb_2O_5 remains stable only at higher oxygen potentials. These results show that Nb may remain in oxide form over a broad interval, but under sufficiently reducing conditions, it may be transferred into non-oxide compounds. The corresponding thermodynamic diagrams are shown in Figure 13.

The Nb–O–Fe subsystem shows that Nb oxides remain stable at relatively high oxygen potentials, whereas the intermetallic $NbFe_2$ becomes thermodynamically favorable only in a much more reducing field. This implies that Fe-bearing metallic or intermetallic Nb hosts are unlikely to dominate under oxidized or moderately oxidized oxide-processing conditions, but may become relevant only after substantial oxygen depletion. Thus, the

thermodynamic data constrain the redox window in which Nb is expected to remain in oxide form rather than to pass into carbide- or intermetallic-bearing states. In the present work, these diagrams are used as equilibrium-based interpretative constraints and not as direct experimental proof of the actual phase identity of every Nb-bearing component in the investigated samples.

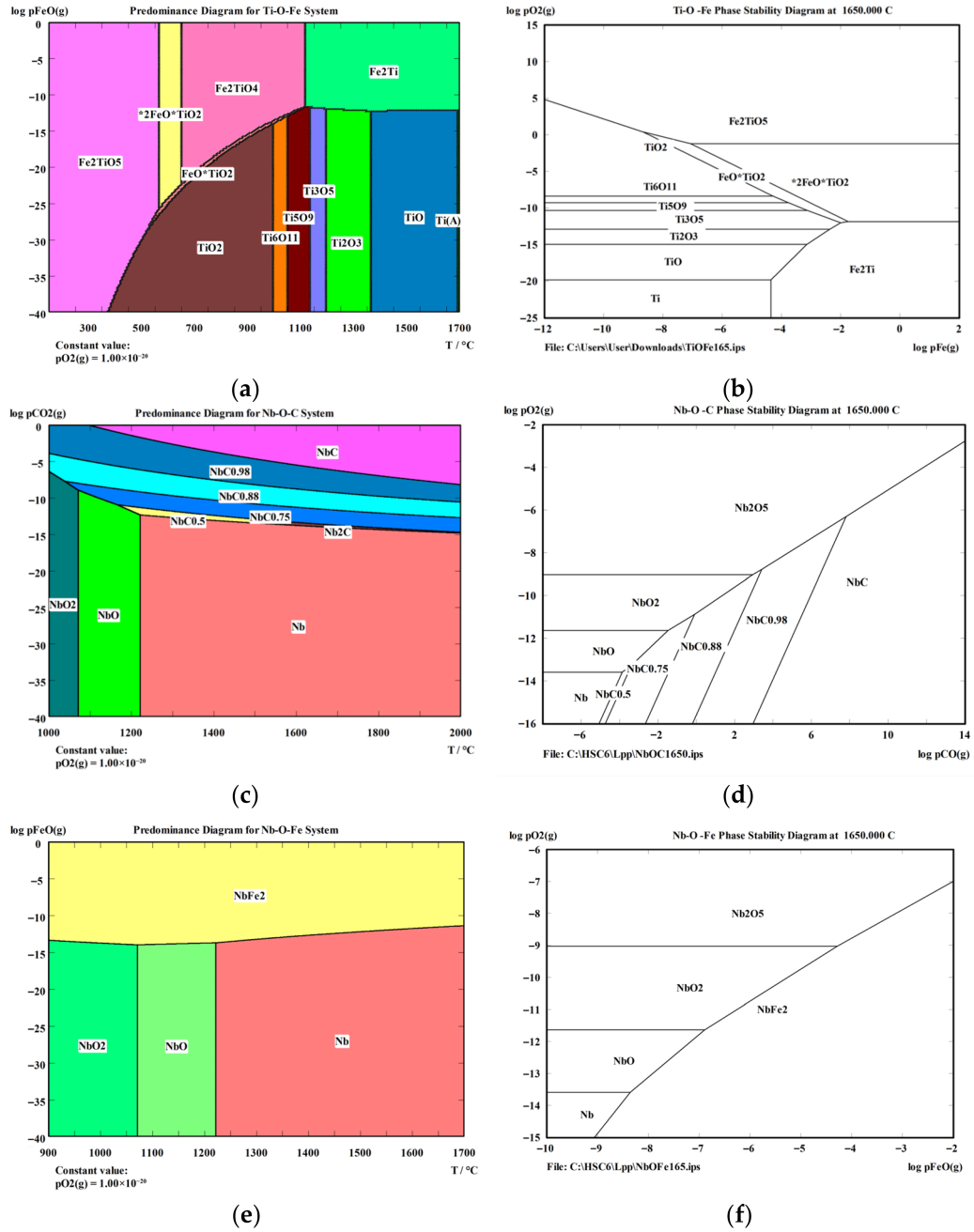


Figure 13. Thermodynamic diagrams illustrating phase-stability relations relevant to Nb redistribution in the Fe–Ti–O system: (**a**) predominance diagram for the Fe–Ti–O system; (**b**) phase-stability diagram for the Ti–O–Fe subsystem at 1600 °C; (**c**) predominance diagram for the Nb–O–C system; (**d**) phase-stability diagram for the Nb–O–C subsystem at 1600 °C; (**e**) predominance diagram for the Nb–O–Fe system; (**f**) phase-stability diagram for the Nb–O–Fe subsystem at 1600 °C.

3.4.2. Thermodynamic Constraints on Nb Redistribution

Taken together, the thermodynamic calculations indicate that Nb redistribution in the investigated systems is controlled by three principal factors: temperature, oxygen potential, and the availability of TiO_2-rich structural hosts. At low Nb contents and under oxide-

stable conditions, Nb is expected to be retained mainly in structurally compatible oxide hosts, first as a trace isomorphic component and then as part of TiO_2-related solid solutions. As temperature increases and local phase reorganization proceeds, the calculations allow progressive redistribution of Nb into more compositionally distinct oxide phases, including niobates and complex Fe–Ti–Nb oxides. Under still more reducing conditions, the stability fields of Nb carbides and $NbFe_2$ become accessible, but these fields lie outside the most probable regime of the natural material studied here. Such non-oxide forms may also become relevant in other strongly reducing processing routes, including metallothermic systems, but these regimes lie outside the principal oxide-processing conditions considered in the present study.

These results are broadly consistent with the experimental interpretation that one probable pathway of Nb evolution in the present Fe–Ti–O systems proceeds from background incorporation in Fe–Ti oxide matrices toward concentration in TiO_2-related domains and, under favorable conditions, toward segregation into discrete Nb-bearing oxide phases. In this sense, the thermodynamic modeling does not contradict the microanalytical and XRD results, but provides an equilibrium-based stability framework that helps explain why TiO_2-rich domains act as the principal concentrators of Nb and why separate niobate phases appear only in the more advanced stage of phase evolution. These relations should be understood as equilibrium-based mechanistic constraints rather than as direct experimental proof of every inferred redistribution step.

4. Discussion

4.1. Two-Mode Distribution of Nb in the Fe–Ti–O System

The combined microanalytical, diffraction, thermal, and thermodynamic data are consistent with the working hypothesis that Nb in the Fe–Ti–O system is distributed in two principal modes rather than in a single structurally uniform form. In the investigated natural ilmenite concentrate, Nb occurs both as a low-level background component in the Fe–Ti oxide matrix and as localized enrichments associated with TiO_2-rich domains, especially rutile lamellae. The mapped background signal, the point analyses of Nb-enriched domains, and the first-order estimate showing that approximately 60–80% of the detected Nb is associated with the lamellar channel together suggest that the principal local Nb concentrators in the studied natural material appear to be TiO_2-rich exsolution or transformation domains rather than the bulk ilmenite matrix itself, but TiO_2-rich exsolution or transformation domains.

This interpretation is consistent with the crystal-chemical behavior of Nb as a heterovalent substituent for Ti in octahedral coordination [9–11]. At low concentrations, Nb can be incorporated into Fe–Ti oxide structures as a trace isomorphic impurity, corresponding to the background matrix mode. In the natural material, this statement refers to the observed room-temperature microstructural state interpreted as the product of prior geological and thermal evolution. In the model systems, the corresponding oxide-stable incorporation is consistent with the investigated 900–1200 °C interval. In chemical terms, this background mode is interpreted as predominantly oxide-bound Nb(V) accommodated in Ti-bearing oxide hosts. However, once TiO_2-rich lamellae or rutile-like domains develop, local redistribution becomes more efficient, and Nb is concentrated preferentially in those structurally favorable domains.

4.2. TiO_2-Rich Domains as the Principal Concentrators of Nb

The natural and model systems together suggest that TiO_2-related domains are the most favorable hosts for local Nb enrichment in the investigated Fe–Ti–O materials. In the natural concentrate, the highest measured Nb values are associated with rutile-like

lamellae, whereas in the model systems the principal Nb-bearing host is interpreted on a semi-quantitative XRD basis as an ilmenorutile-like phase. Accordingly, local Nb maxima in Fe–Ti–O systems are controlled not only by bulk Nb abundance, but also by the development of TiO_2-rich microdomains during textural evolution. This conceptual evolution of Nb occurrence in the Fe–Ti–O system is summarized in Figure 14.

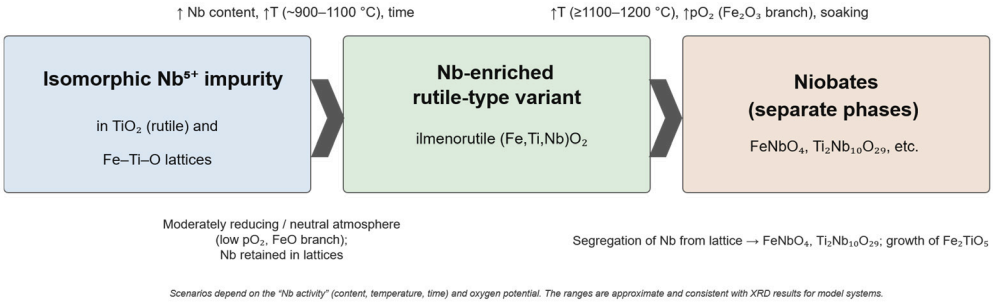


Figure 14. Conceptual evolution of Nb occurrence in the Fe–Ti–O system as a function of increasing temperature, oxygen potential, and holding time: transition from low-level isomorphic Nb impurity in TiO_2- and Fe–Ti–O lattices to Nb-enriched rutile-type variants (ilmenorutile-like solid solutions) and, under more advanced redistribution conditions, to separate niobate phases.

4.3. Crystal-Chemical Mechanism of Nb Incorporation and Charge Compensation

The natural and model data are also consistent with a crystal-chemical interpretation in which Nb is initially incorporated into Ti-bearing oxide lattices by substitution in Ti sites. At the background level, this corresponds to heterovalent substitution of Nb(V) for Ti(IV), which requires local charge compensation [9–11]. This substitution is crystal-chemically plausible because the ionic radii of octahedrally coordinated Nb(V) and Ti(IV) are close, commonly cited as about 0.64 Å and 0.605 Å, respectively. In Fe–Ti oxide matrices and TiO_2-related phases, such compensation may proceed through coupled substitutions involving Fe oxidation-state changes and/or cation-vacancy mechanisms. Although the present study is not based on atomically resolved crystallographic refinement, the observed phase evolution, the behavior of rutile-like domains, and the persistence of ilmenorutile-like hosts in the model systems are all consistent with this general substitutional mechanism. This crystal-chemical interpretation is summarized schematically in Figure 15.

The importance of this mechanism is that it links trace structural incorporation and later-stage microphase enrichment within one continuous framework. Nb does not need to appear immediately as a separate phase. It may first be retained in Ti-bearing lattice positions, then progressively partition into TiO_2-rich domains as those domains evolve texturally and thermodynamically, and only later, under favorable conditions, segregate into more compositionally distinct Nb-bearing oxide phases. Accordingly, the crystal-chemical substitution mechanism provides one plausible starting point for the broader evolutionary sequence proposed here.

4.4. Integration of Natural, Model, and Thermodynamic Evidence

The present study integrates three converging lines of evidence: microanalytical observations on the natural ilmenite concentrate, phase and thermal behavior of the model TiO_2–FeO–Nb_2O_5 and TiO_2–Fe_2O_3–Nb_2O_5 systems, and thermodynamic constraints derived from HSC calculations. Together, these datasets are consistent with a coherent evolutionary model of Nb behavior in the Fe–Ti–O system.

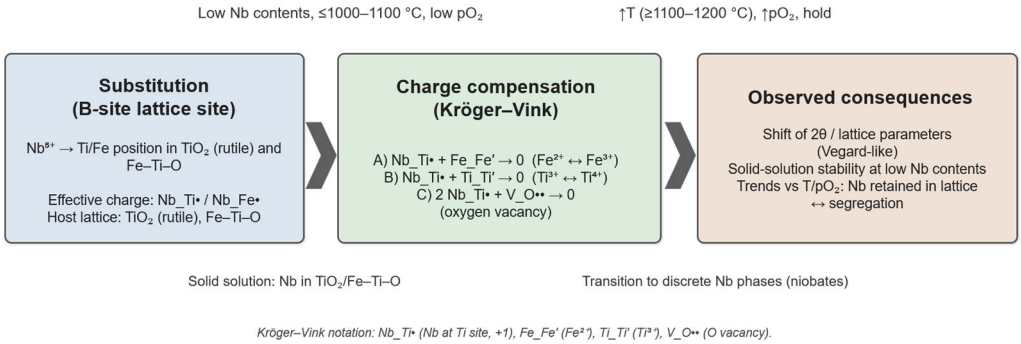


Figure 15. Crystal-chemical interpretation of Nb incorporation in Fe–Ti–O phases: substitution of Nb in Ti sites, possible charge-compensation mechanisms in Kröger–Vink notation, and the resulting evolution from solid-solution incorporation to local enrichment and phase segregation.

The natural material demonstrates that the redistribution of Nb is already strongly heterogeneous at the grain scale, with local Nb enrichment linked to rutile lamellae and rutile-like microdomains. The model systems show that under controlled thermal treatment Nb is preferentially stabilized in ilmenorutile-like phases and, at more advanced stages of phase evolution, in additional Nb-bearing oxides tentatively assigned on a semi-quantitative XRD basis, including $FeNbO_4$, Ti niobates, and complex Fe–Ti–Nb oxides. The thermodynamic results presented in Figure 13 provide the phase-stability framework needed to interpret these observations. In the Fe–Ti–O subsystem, TiO_2 and Ti-rich Fe–Ti oxides remain stable over wide ranges of temperature and oxygen potential, defining the main oxide framework in which Nb redistribution occurs. In the Nb–O–C and Nb–O–Fe subsystems, the calculations show that oxide forms of Nb remain stable over broad intervals, whereas carbide-bearing and intermetallic Nb hosts become favorable only under much more reducing conditions than those most likely represented by the investigated natural object.

This comparison helps explain why the natural material is dominated by background and lamellar Nb rather than by abundant discrete niobates, while the synthesized model systems already show the appearance of such phases. The two sets of observations can be interpreted as representing different positions along the same evolutionary pathway. The formation of discrete niobates and related Nb-bearing oxide phases becomes more probable at elevated temperature, under oxide-stable conditions, and where sufficient local Nb activity and phase reorganization permit redistribution from TiO_2-related solid-solution hosts into more compositionally distinct oxide assemblages. In the present study, such niobate formation refers primarily to Ti-bearing niobate-type and related complex oxide assemblages identified on a semi-quantitative XRD basis. The natural concentrate records a stage at which microphase enrichment in TiO_2-rich domains is well developed, whereas the model systems represent higher-Nb-activity and thermally driven conditions under which segregation into distinct Nb-bearing oxide phases becomes experimentally observable. This integrated comparison should therefore be understood as a convergent interpretative framework rather than as direct experimental proof of every individual step in the inferred Nb redistribution pathway. The integrated interpretation of these stages and regimes is summarized in Table 11.

Table 11. Integrated interpretation of Nb redistribution in the Fe–Ti–O system based on natural observations, model systems, and thermodynamic constraints.

Stage/Regime	Nb Host	Evidence	Interpretation
Low Nb content; weak textural differentiation	Background isomorphic Nb in Fe–Ti oxide matrix	Matrix point analyses; low integrated Nb in maps	Initial trace Nb occurrence interpreted as consistent with background incorporation
Formation of TiO_2-rich lamellae or rutile-like domains	Nb-enriched rutile-like microdomains/lamellar channel	BSE images; EDS of lamellae; 60–80% Nb in lamellar channel	Main concentration stage identified in representative analyzed grains
Oxide-stable regime (~1100–1200 °C)	Ilmenorutile-like solid solution $(Ti,Fe,Nb)O_2$	XRD and thermal analysis of model systems	Principal Nb host interpreted on a semi-quantitative XRD basis in model oxide systems
Advanced phase reorganization	Tentatively assigned niobates and complex Fe–Ti–Nb oxides	Semi-quantitative XRD evidence consistent with $FeNbO_4$, Ti niobates, and complex Fe–Ti–Nb oxides	Late-stage Nb segregation
Strongly reducing conditions	Nb carbides or $NbFe_2$	Thermodynamic diagrams for Nb–O–C and Nb–O–Fe	Thermodynamically possible, but not inferred to dominate under the principal conditions considered here

4.5. Temperature Window and Redox Dependence of Nb-Bearing Phases

The thermal and diffraction results indicate that the interval 1100–1200 °C appears to be the most favorable for stabilization of Nb-bearing oxide assemblages in the investigated model systems. In the FeO branch, the most pronounced thermal instability is observed near 1000 °C, whereas samples synthesized at 1100 and 1200 °C display markedly more stable behavior. This instability is consistent with incomplete phase stabilization at this stage and with ongoing redistribution among rutile-oriented and Fe-bearing oxide components, rather than with formation of a single fully stabilized Nb host. In the Fe_2O_3 branch, the progression toward stable assemblages is smoother, and the 1200 °C samples show the highest thermal resistance. These observations are consistent with the XRD data, which indicate that ilmenorutile-like phases persist over a wide temperature interval, while additional Nb-bearing oxides appear as phase evolution proceeds. Taken together, these relations are interpreted as comparative indicators of phase-stability evolution rather than as fully quantitative phase determinations.

The comparison between the FeO- and Fe_2O_3-based systems also shows that Nb redistribution is coupled to the redox evolution of the Fe-bearing oxide subsystem. In both model systems, TiO_2-related phases remain important Nb hosts, but the balance between solid-solution retention and segregation into additional phases differs. The Fe_2O_3-based branch shows a stronger tendency toward progressive pseudobrookite development and associated Nb-bearing phase evolution with increasing temperature, whereas the FeO-based branch preserves a more rutile-dominant character over a broader interval. Thus, although the TiO_2 subsystem remains the principal domain of Nb concentration in the investigated systems, the final mineralogical form in which Nb is retained is controlled by the broader Fe–Ti–O phase relations and their redox-dependent evolution. In this sense, temperature and redox state are interpreted here as governing physicochemical controls on

Nb-host evolution, not as isolated variables acting independently of the phase assemblage as a whole.

4.6. Methodological Limitations and Interpretative Boundaries

The proposed mechanistic model should be considered together with several methodological limitations. Most importantly, the estimate that approximately 60–80% of the detected Nb is associated with the lamellar channel is a first-order two-dimensional approximation derived from area-based domain analysis combined with local semi-quantitative EDS data; it is not a rigorous stereological reconstruction of the full three-dimensional Nb budget, and no formal propagated uncertainty was calculated. In addition, matrix Nb commonly occurs near the practical interpretative limit of SEM-EDS, so weak or near-zero values must be treated conservatively. The Nb-enriched lamellar domains are therefore described here as rutile-like or rutile-related rather than crystallographically resolved pure rutile, and minor phases indicated by weak XRD reflections are treated cautiously. Accordingly, the central conclusions are based on the convergence of microanalytical, diffraction, thermal, and thermodynamic evidence rather than on any single weak phase assignment or analytically fragile local Nb value.

4.7. Implications for Fe–Ti–O Materials and Future Work

The present study provides an interpretative framework in which Nb in Fe–Ti–O systems is treated as an element redistributed through structurally and texturally controlled states linking low-level incorporation, TiO_2-controlled enrichment, and possible later-stage segregation. Future work should focus on higher-resolution characterization of Nb-enriched lamellar domains and on more systematic high-sensitivity microanalytical datasets for refining the interpretation of low-level background Nb occurrence.

5. Conclusions

The present study is consistent with the interpretation that Nb in the Fe–Ti–O system is distributed in two principal modes: as a low-level isomorphic impurity in the Fe–Ti oxide matrix and as localized enrichments in TiO_2-rich domains, especially rutile lamellae. In the investigated natural ilmenite concentrate, the lamellar channel represents the dominant pathway of local Nb concentration, and first-order empirical area-based estimates suggest that approximately 60–80% of the detected Nb is associated with rutile lamellae or rutile-like microdomains within representative analyzed grains and sections.

The model TiO_2–FeO–Nb_2O_5 and TiO_2–Fe_2O_3–Nb_2O_5 systems indicate on a semi-quantitative XRD basis that the principal Nb-bearing host over a broad temperature interval is an ilmenorutile-like solid solution, whereas further phase evolution at elevated temperature is accompanied by the appearance of additional Nb-bearing oxides tentatively assigned on a semi-quantitative XRD basis. These results are consistent with the interpretation that TiO_2-related domains act as the principal loci of Nb concentration in the investigated materials and that redistribution progresses from trace structural incorporation toward phase-selective enrichment and segregation.

Thermal and diffraction data show that the interval 1100–1200 °C is the most favorable for stabilization of Nb-bearing oxide assemblages in the model systems. Thermodynamic modeling further constrains this behavior by showing that oxide forms of Nb remain stable over broad temperature–oxygen-potential ranges, whereas carbide-bearing and intermetallic Nb hosts become favorable only under substantially lower oxygen potentials, typically promoted by higher temperature and/or stronger reductant availability, including higher effective carbon activity in the Nb–O–C framework, than those most likely represented by the investigated natural object.

Taken together, the natural observations, model experiments, and thermodynamic calculations are consistent with a coherent mechanistic framework in which Nb evolution proceeds from low-level incorporation to TiO_2-related enrichment and, under favorable conditions, to segregation into distinct Nb-bearing oxides or niobates. This mechanistic framework may assist in the interpretation of Nb behavior in natural and technological Fe–Ti–O materials.

Author Contributions: Conceptualization, T.K.S.; methodology, T.K.S.; validation, T.K.S., T.A.C., R.K.S., N.B. and Y.S.M.; formal analysis, T.K.S. and T.A.C.; investigation, R.K.S., N.B. and Y.S.M.; resources, T.K.S.; data curation, R.K.S., N.B. and Y.S.M.; writing—original draft preparation, T.K.S.; writing—review and editing, T.K.S. and T.A.C.; visualization, T.K.S.; supervision, T.K.S.; project administration, T.K.S. All authors have read and agreed to the published version of the manuscript.

Funding: This research was funded by the Science Committee of the Ministry of Science and Higher Education of the Republic of Kazakhstan, grant No. AP22686490.

Data Availability Statement: The data presented in this study are available on request from the corresponding author. The data are not publicly available because they form part of an ongoing research project.

Acknowledgments: During the preparation of this manuscript, the authors used ChatGPT (OpenAI, GPT-5.4 Thinking) for language refinement, translation, structural editing, and improvement of textual clarity. The authors reviewed and edited the output and take full responsibility for the content of this publication.

Conflicts of Interest: Author Turar Kusmanovich Sarsembekov was employed by the company BioMin Tech LLP. The remaining authors declare that the research was conducted in the absence of any commercial or financial relationships that could be construed as a potential conflict of interest.

Abbreviations

The following abbreviations are used in this manuscript:

BSE	Backscattered Electron
DTA	Differential Thermal Analysis
DTG	Derivative Thermogravimetry
EDS	Energy-Dispersive Spectroscopy
EPMA	Electron Probe Microanalysis
HFSE	High-Field-Strength Element
HSC	HSC Chemistry
ICDD	International Centre for Diffraction Data
PDF-2	Powder Diffraction File Database
SEM	Scanning Electron Microscopy
TG	Thermogravimetry
WDS	Wavelength-Dispersive Spectroscopy
XRD	X-ray Diffraction

References

1. Buddington, A.F.; Lindsley, D.H. Iron-titanium oxide minerals and synthetic equivalents. *J. Petrol.* **1964**, *5*, 310–357. [CrossRef]
2. Spencer, K.J.; Lindsley, D.H. A solution model for coexisting iron-titanium oxides. *Am. Mineral.* **1981**, *66*, 1189–1201.
3. Andersen, D.J.; Lindsley, D.H. Internally consistent solution models for Fe–Mg–Mn–Ti oxides: Fe–Ti oxides. *Am. Mineral.* **1988**, *73*, 714–726.
4. Ghiorso, M.S.; Sack, R.O. Fe–Ti oxide geothermometry: Thermodynamic formulation and the estimation of intensive variables in silicic magmas. *Contrib. Mineral. Petrol.* **1991**, *108*, 485–510. [CrossRef]
5. Ghiorso, M.S.; Evans, B.W. Thermodynamics of rhombohedral oxide solid solutions and a revision of the Fe–Ti two-oxide geothermometer/oxygen-barometer. *Am. J. Sci.* **2008**, *308*, 957–1039. [CrossRef]

6. Andersen, D.J.; Lindsley, D.H.; Davidson, P.M. QUILF: A Pascal program to assess equilibria among Fe–Mg–Mn–Ti oxides, pyroxenes, olivine, and quartz. *Comput. Geosci.* **1993**, *19*, 1333–1350. [CrossRef]
7. Lepage, L.D. ILMAT: An Excel worksheet for ilmenite-magnetite geothermometry and oxygen barometry. *Comput. Geosci.* **2003**, *29*, 673–678. [CrossRef]
8. Yavuz, F. WinMIgob—A Windows program for ilmenite-magnetite geothermometry and oxygen barometry. *J. Geosci.* **2021**, *66*, 51–69. [CrossRef]
9. Černý, P.; Ercit, T.S. Mineralogy of niobium and tantalum: Crystal chemical relationships, paragenetic aspects and their economic implications. In *Lanthanides, Tantalum and Niobium*; Springer: Berlin, Germany, 1989; pp. 27–79.
10. Nakashima, K.; Imaoka, T. Niobian and zincian ilmenites in syenites from Cape Ashizuri, Southwest Japan. *Mineral. Petrol.* **1998**, *63*, 1–17. [CrossRef]
11. Chakhmouradian, A.R.; Mitchell, R.H. Niobian ilmenite, hydroxylapatite and sulfatian monazite: Alternative hosts for incompatible elements in calcite kimberlite from Internatsional'naya, Yakutia. *Can. Mineral.* **1999**, *37*, 1177–1189.
12. Meinhold, G. Rutile and its applications in earth sciences. *Earth-Sci. Rev.* **2010**, *102*, 1–28. [CrossRef]
13. Zack, T.; von Eynatten, H.; Kronz, A. Trace element abundances in rutile from eclogites and associated garnet mica schists. *Chem. Geol.* **2002**, *184*, 97–122. [CrossRef]
14. Foley, S.F.; Barth, M.G.; Jenner, G.A. Rutile/melt partition coefficients for trace elements and implications for subduction zone magmas. *Geochim. Cosmochim. Acta* **2000**, *64*, 933–938. [CrossRef]
15. Klemme, S.; Prowatke, S.; Hametner, K.; Günther, D. Partitioning of trace elements between rutile and silicate melts: Implications for subduction zones. *Geochim. Cosmochim. Acta* **2005**, *69*, 2361–2371. [CrossRef]
16. Lueder, M.; Tamblyn, R.; Rubatto, D.; Lanari, P.; Markmann, T.A.; Hermann, J. Intra-grain variability of hydrogen and trace elements in rutile. *Chem. Geol.* **2024**, *671*, 122480. [CrossRef]
17. Grey, I.E.; Reid, A.F. The structure of pseudorutile and its role in the natural alteration of ilmenite. *Am. Mineral.* **1975**, *60*, 898–906.
18. Mücke, A.; Bhadra Chaudhuri, J.N. The continuous alteration of ilmenite through pseudorutile to leucoxene. *Ore Geol. Rev.* **1991**, *6*, 25–44. [CrossRef]
19. He, P.-L.; Huang, X.-L.; Zhang, L. High-precision measurement of trace-level Nb, Sn, Ta, and W in rutile using electron probe microanalysis. *Solid Earth Sci.* **2024**, *9*, 100197. [CrossRef]
20. Cook, N.J.; Ciobanu, C.L.; Meria, D.; Silcock, D.; Wade, B. Trace element analysis of minerals in magmatic and hydrothermal systems. *Minerals* **2016**, *6*, 111. [CrossRef]
21. Bollaert, Q.; Chassé, M.; Morin, G.; Baptiste, B.; Courtin, A.; Galoisy, L.; Landrot, G.; Quantin, C.; Calas, G. Atomic-scale environment of niobium in ore minerals as revealed by XANES and EXAFS at the Nb K-edge. *Eur. J. Mineral.* **2024**, *36*, 55–72. [CrossRef]
22. Droop, G.T.R. A general equation for estimating Fe^{3+} concentrations in ferromagnesian silicates and oxides from microprobe analyses, using stoichiometric criteria. *Mineral. Mag.* **1987**, *51*, 431–435. [CrossRef]
23. Coint, N.; Mansur, E.T.; Keiding, J.K.; Skår, Ø. Trace elements in ilmenite, titanomagnetite and apatite unravel the petrogenesis of Fe–Ti–P-(+/-Zr) rich rocks and associated nelsonite from the Raftsund intrusion, Vesterålen-Lofoten AMCG suite, Northern Norway. *Lithos* **2023**, *460–461*, 107389. [CrossRef]
24. Tomkins, H.S.; Powell, R.; Ellis, D.J. The pressure dependence of the zirconium-in-rutile thermometer. *J. Metamorph. Geol.* **2007**, *25*, 703–713. [CrossRef]
25. Xiong, X.; Keppler, H.; Audétat, A.; Ni, H.; Sun, W.; Li, Y. Partitioning of Nb and Ta between rutile and felsic melt and the fractionation of Nb/Ta during partial melting of hydrous metabasalt. *Geochim. Et Cosmochim. Acta* **2011**, *75*, 1673–1692. [CrossRef]
26. Schmidt, M.W.; Dardon, A.; Chazot, G.; Vannucci, R. The dependence of Nb and Ta rutile–melt partitioning on melt composition and Nb/Ta fractionation during subduction processes. *Earth Planet. Sci. Lett.* **2004**, *226*, 415–432. [CrossRef]
27. Pearce, N.J.G. Niobium-bearing ilmenites. *Mineral. Mag.* **1990**, *54*, 451–456.
28. McEnroe, S.A.; Robinson, P.; Langenhorst, F.; Frandsen, C.; Terry, M.P.; Boffa Ballaran, T. Magnetization of exsolution intergrowths of hematite and ilmenite: Mineral chemistry, phase relations, and magnetic properties of hemo-ilmenite ores with micron- to nanometer-scale lamellae from Allard Lake, Quebec. *J. Geophys. Res.* **2007**, *112*, B10103. [CrossRef]
29. Frandsen, C.; Madsen, D.E.; Salazar-Alvarez, G.; Kongsdal, A.; Bøjesen, A.; Christiansen, T.L.; Keller, L.; Andersen, N.H.; Mørup, S. Magnetic interaction and exsolution microstructures in hemo-ilmenite: Nanoscale evidence. *Phys. Rev. B* **2010**, *82*, 214422. [CrossRef]
30. Kuganathan, N.; Srikaran, R.; Fossati, P.C.M.; Chroneos, A. Theoretical modeling of defects, dopants, and diffusion in the mineral ilmenite. *Minerals* **2019**, *9*, 610. [CrossRef]

Disclaimer/Publisher's Note: The statements, opinions and data contained in all publications are solely those of the individual author(s) and contributor(s) and not of MDPI and/or the editor(s). MDPI and/or the editor(s) disclaim responsibility for any injury to people or property resulting from any ideas, methods, instructions or products referred to in the content.